Earth and Planetary Science Letters 395 (2014) 1–12

Contents lists available at ScienceDirect

Earth and Planetary Science Letters

www.elsevier.com/locate/epsl

Decadal persistence of cycles in lava lake motion at Erebus volcano, Antarctica

Nial Peters [a,*], Clive Oppenheimer [a], Philip Kyle [b], Nick Kingsbury [c]

[a] Department of Geography, University of Cambridge, Downing Place, Cambridge, CB2 3EN, UK
[b] Department of Earth and Environmental Science, New Mexico Institute of Mining and Technology, Socorro, NM 87801, USA
[c] Department of Engineering, University of Cambridge, Trumpington Street, Cambridge, CB2 1PZ, UK

ARTICLE INFO

Article history:
Received 9 December 2013
Received in revised form 13 March 2014
Accepted 15 March 2014
Available online 3 April 2014
Editor: J. Brodholt

Keywords:
lava lake
thermal imaging
convection
bidirectional flow
conduit
Erebus volcano

ABSTRACT

Studies of Erebus volcano's active lava lake have shown that many of its observable properties (gas composition, surface motion and radiant heat output) exhibit cyclic behaviour with a period of ~10 min. We investigate the multi-year progression of the cycles in surface motion of the lake using an extended (but intermittent) dataset of thermal infrared images collected by the Mount Erebus Volcano Observatory between 2004 and 2011. Cycles with a period of ~5–18 min are found to be a persistent feature of the lake's behaviour and no obvious long-term change is observed despite variations in lake level and surface area. The times at which gas bubbles arrive at the lake's surface are found to be random with respect to the phase of the motion cycles, suggesting that the remarkable behaviour of the lake is governed by magma exchange rather than an intermittent flux of gases from the underlying magma reservoir.

1. Introduction

Persistently active lava lakes are a spectacular but rare form of open-vent volcanism found at only a handful of volcanoes around the world. An active lava lake is the exposed top of a volcano's magmatic plumbing system. Longevity of such lakes has been argued to reflect either effective transfer of magma between the lake and the deeper system (e.g. Oppenheimer et al., 2004; Francis et al., 1993), or a supply of gas bubbles from depth (Witham and Llewellin, 2006; Bouche et al., 2010). It can be shown experimentally that processes occurring at depth will manifest themselves at the surface as changes in the lake's behaviour, for example its surface level (Witham et al., 2006) or gas flux (Divoux et al., 2009). It follows therefore, that observations of lake properties can yield valuable insights into the processes occurring at depth in the magmatic system, where direct measurements are not possible. This link with the deeper magmatic system makes the study of active lava lakes (sensu Tilling, 1987) of particular importance.

Erebus is a 3794-m-high stratovolcano located on Ross Island, Antarctica. It is often claimed to be the southernmost active volcano in the world and is known to have hosted an active phonolite lava lake since at least 1972 (Giggenbach et al., 1973). Although other small lakes have appeared intermittently over this period, the main, "Ray" lake, has been a permanent feature of the crater throughout (with the notable exception of 1984–1985 when it was buried following sustained explosive eruptions) (Kyle et al., 1990).

The stable convective behaviour of the Erebus lava lake is punctuated by intermittent (De Lauro et al., 2009) Strombolian eruptions associated with the rupture of large (decametric) gas bubbles at the lake surface (Dibble et al., 2008; Gerst et al., 2013). Phases of increased and more intense Strombolian activity (several explosions per day, with ejecta escaping the main crater) recur, lasting 1–10 months and are followed by more extended intervals during which gas bubble bursts are less frequent and of a smaller size (a few explosions per week, with all ejecta being confined to the crater – see for example Jones et al. (2008)). The chemical and mineralogical composition of erupted lavas has remained constant for approximately 17 ka and the abundance of unusually large anorthoclase crystals is indicative of sustained shallow magma convection throughout this period (Kelly et al., 2008). Indeed, the presence of such large crystals may be a significant influence on the behaviour of the shallow convection at Erebus (Molina et al., 2012). Other properties of the lake also demonstrate remarkably consistent long-term behaviour, for example SO_2 flux (Sweeney et al., 2008) and radiant heat output (Wright and Pilger, 2008).

On shorter time scales, many of the lake's properties exhibit a pronounced pulsatory behaviour. Oppenheimer et al. (2009) observed that the radiative heat loss, surface velocity and certain

* Corresponding author.
E-mail address: njp39@cam.ac.uk (N. Peters).

http://dx.doi.org/10.1016/j.epsl.2014.03.032

magmatic gas ratios all oscillated with a period of ∼10 min. The cycles appeared to be phase locked with each other, suggesting a common mechanism was responsible for the oscillations in each property. Evidence of similar cyclicity has also been observed in the SO_2 flux (Boichu et al., 2010), and the H_2/SO_2 ratio (Moussallam et al., 2012), but these have yet to be linked definitively to the cycles observed by Oppenheimer et al. (2009).

One possible explanation for the observed behaviour is pulsatory exchange flow of hot, degassing magma into the lake from the subjacent conduit. It has been shown experimentally that given two liquids flowing in opposite directions in a vertical pipe (for example driven by a density difference between them), under certain flow conditions an instability occurs which results in a pulsed flow (Huppert and Hallworth, 2007). Oppenheimer et al. (2009) suggested that such behaviour may explain the cycles at Erebus volcano, with bubbly and degassing, low density magma rising up the conduit into the lake whilst degassed, denser magma sinks back down the conduit again. The resulting pulsatory flow delivers packets of fresh magma into the lake quasi-periodically, giving rise to the observed cycles in lake properties. The period of the cycles would be expected to reflect the rheological properties and velocity of the bubbly flow and geometry of the conduit.

The previous studies at Erebus have analysed only very short time-series of data (circa 1 h), and no investigation of the long-term behaviour of the cycles has yet been conducted. However, thermal infrared (IR) images of the Erebus lava lake have been collected almost every year since 2004 during the Mount Erebus Volcano Observatory's annual austral summer field campaigns. Using a similar technique to that of Oppenheimer et al. (2009), we have extracted mean surface speed estimates from the usable portions of the now substantial IR dataset. Using the mean surface speed as a proxy to assess the cyclicity of the lake motion, we present an overview of its behaviour between 2004 and 2011 and compare this to visible changes in the lake's appearance. Using a dataset recorded at higher time resolution in 2010, we identify times when bubbles arrive at the surface of the lake and compare this to the phase of the cycles.

Our specific aims are to identify the persistence (or otherwise) of the cyclic behaviour within and between field seasons; to search for any variability in cycle length that might point to changes in lake/conduit configuration or rheological characteristics of the magma; and to probe further the origins of the remarkable cyclic behaviour of the lava lake. We also compare observations at Erebus with those for other active lava lakes.

2. Summary of activity

In the following analyses, data from field campaigns between 2004 and 2011 have been used. Although the general behaviour of the lava lake at Erebus is fairly consistent from year to year, there are some observable variations. It is therefore important to set the results presented here within the context of the state of activity of the lake during each of the respective field campaigns.

During the 2004 field season, there were two separate lava lakes present in the crater (Calkins et al., 2008). By the 2005 field season, only the "Ray" lake remained (Davies et al., 2008), and no additional lakes have since been observed. All data presented here are from the "Ray" lake, and henceforth, we refer to it simply as the lava lake.

Fig. 1 shows how the visible surface area of the lava lake has changed throughout the period of study. Possible reasons for this change are discussed in detail in Section 4. Despite the reduction in visible surface area from 2004 onwards, there have been no other apparent changes in the behaviour of the lava lake. Stable convective behaviour has been maintained throughout. This is characterised by the lateral migration of cracks in the lake's crust

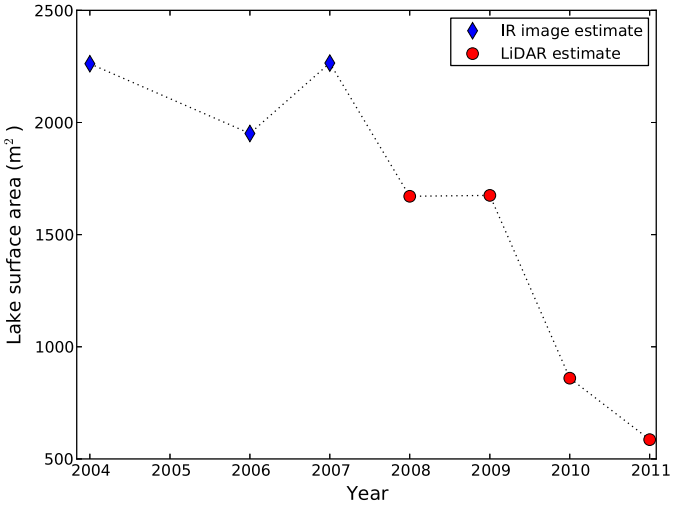

Fig. 1. Surface area of the Erebus lava lake by field season (i.e. December of the year shown). The areas have been estimated from a combination of terrestrial laser scan data (Jones, 2013, Frechette and Killingsworth, pers. comm.) and rectified IR images.

across the surface. These typically move radially outwards from the approximate centre of the lake, but more complex flow patterns with several "convection cells" and abrupt reversals of flow direction are also common. Lobes of fresh lava are occasionally observed to spread across the surface of the lake from upwelling regions, and there is visible subduction of the surface crust at the downwelling regions. These behaviours are all evident in the animation provided in the supplementary material for the electronic version of this manuscript.

Bubbles of a variety of sizes are observed to surface in the lake. We describe bubbles as "large" if they result in significant ejection of material from the lake. Such bubbles (e.g. Fig. 8) are typically 10–30 m in diameter and cause a visible emptying of the lake. We classify such events as being distinct from the far more frequently occurring "small", metre and sub-metre scale bubbles (e.g. panel (d) in Fig. 5) which arrive at the surface of the lake, but do not rupture violently.

A study of explosive events (due to large bubbles) between 2003–2011 using seismic data (Knox, 2012) shows that, with the notable exception of the period from late 2005 to early 2007, their frequency has remained fairly constant at a few per week, with ejecta being entirely confined to the crater. During 2005–2007 however, there were several explosions per day, often of sufficient magnitude to propel ejecta out of the crater, the frequency of these events then gradually declined and by the 2007 field season the lake had returned to its more typical level of activity.

3. Methodology

Fieldwork on Erebus volcano is limited to the austral summer, and typically takes place from late-November to early January. Where we refer to a field season by year, we are referring to the year in which it began. The logistics involved in reaching the crater rim, combined with frequent bad weather conspire to limit the interval of IR image data acquisition to a few weeks each year. The intervals of useful data are further reduced due to fluctuations in the IR transmission between camera and lava lake. When the gas/aerosol plume is highly condensed (high relative humidity) the IR transmission in the camera waveband is poor and the images of the lake are of unusable quality. The latest IR camera system, which was deployed in December 2012, is capable of year-round operation (dependent on power) (Peters et al., 2014). The data from this fully automated system will be analysed in future work.

3.1. Camera hardware

All IR images of the Erebus lava lake used in this study were recorded by tripod-mounted camera systems installed at the Shackleton's cairn site on the northern side of the Main Crater. Three different IR camera systems have been used on Erebus since 2004. The first of these was an Agema Thermovision 550 mid-infrared (3–5 μm) camera, as described by Oppenheimer et al. (2004), which acquired images with a 4 s time-step. The second was a FLIR P25 camera equipped with a 72 mm IR lens. This camera has an uncooled 320 × 240 element detector with a waveband of 7.5–13 μm and a spatial resolution (instantaneous field of view) of 0.31 mrad. The low temperatures at the crater rim of Erebus severely impacted the P25's ability to write images to its compact flash card, and as a result the interval between successive images varies between 8 and 20 s. The most recent IR camera model we have employed is a FLIR SC645, with an uncooled 640 × 480 element detector, waveband of 7.5–13 μm, and a spatial resolution of 0.69 mrad. Although the SC645 is capable of frame rates of up to 25 Hz, we have typically acquired images at 2 s intervals. It was, however, operated with a 0.5 s time-step in acquisitions for a part of the 2010 field season and we have used these higher time resolution data for bubble event analysis (Section 3.5).

3.2. Data selection

Interruptions to the recording of IR images on Erebus are common. The Agema and P25 cameras both required their memory cards to be changed regularly and equipment failure was frequent due to the harsh operating conditions. These factors have resulted in a segmented data set with many gaps. The first step in data selection was to split the data into groups of continuous acquisition that contained no two images more than 40 s apart. Groups spanning less than one hour of acquisition were discarded. Subsequent data processing was performed on a per group basis.

High winds at the summit of Erebus cause camera shake, potentially introducing large errors into the velocity estimates calculated by the motion tracking algorithm. This problem is particularly acute in data from the Agema and P25 cameras, which did not have such stable tripod mounts as does the new SC645 system. Attempted stabilisation of the images in post-processing failed due to the lack of distinctive stationary features in the images. Instead, a simpler approach was followed, in which only periods of data with little or no camera shake were analysed. Due to the large volume of available data, an automated routine for identifying such periods was developed. This involved first defining the bounding box of the lake in each image by thresholding the image at a predetermined level, and identifying the non-zero region. Images in which the bounding box could not be found, or was unusually small were rejected, as these characteristics point to poor visibility of the lake (typically caused by high relative humidity, blowing snow, or rime-ice accumulation on the lens). The centre coordinates of the bounding boxes were then assigned to clusters using SciPy's *fclusterdata* function (Jones et al., 2001). To reduce the run time of the clustering algorithm, duplicate bounding box positions were discarded before clusters were computed. Using the standard deviation of the bounding box coordinates in each cluster as an indicator of camera shake, the best clusters for each year (typically with a standard deviation of <1.0 pixels) were selected. As a final check of data quality, the images in each cluster were compiled into a video, which was then viewed to ensure good visibility of the lake and minimal camera shake throughout.

3.3. Motion tracking

Since the focal plane of the thermal camera is not parallel to the surface of the lava lake, perspective effects mean that each pixel in the image represents a different distance in the plane of the lake. To correct for this distortion, each image was rectified before the motion tracking was carried out. The required transformation was calculated by matching points in the image to points in a terrestrial laser scan of the lake. OpenCV's (Bradski, 2000) *cvFindHomography* function was then used to calculate the required transformation matrix, and the *cvWarpPerspective* function used to apply it (see Bradski and Kaehler, 2008). Correcting the images in this way also accounts for any lens distortion. Terrestrial laser scan data of the lava lake were only available for 2008 onwards. For thermal images from earlier years, the homography matrix was calculated from the viewing angle of the camera and the size of the lake (which had been estimated with a handheld laser range finder). Although this method neglects lens distortion, we expect the effects to have little impact on the results obtained.

The significant temperature contrast between the lake and the surrounding crater causes problems for the feature tracking algorithm. As the strongest feature in the image, the lake boundary tends to dominate over the structure within the lake that we are actually interested in. This issue can be overcome by masking the regions outside of the lake with Gaussian-distributed white noise with a mean and variance similar to that of the pixels within the lake. Random noise is used rather than a fixed value to prevent the output of the bandpass filters used in the wavelet decomposition from being exactly zero, as this causes the algorithm to fail.

The feature tracking algorithm itself is based on the Dual-Tree Complex Wavelet Transform (DT-$\mathbb{C}$WT) (Kingsbury, 2001). Unlike the widely used Discrete Wavelet Transform (DWT) (see for example Polikar, 2010), DT-$\mathbb{C}$WT is approximately shift invariant, meaning that shifts in input signal do not cause changes in energy distribution between wavelet coefficients at different scales. Instead, it is found that shifts in the input signal manifest themselves as a phase shift between the wavelet coefficients. By decomposing each frame in a series of images using the DT-$\mathbb{C}$WT and comparing the phase shifts between the subimages, it is possible to estimate the displacement field that maps features in one frame to the next. The estimate is first made at a coarse level of decomposition, with subsequent estimates made at finer levels so as to refine the result (Magarey and Kingsbury, 1998). Oppenheimer et al. (2009) tuned the method specifically for working with IR images from Erebus volcano, and we adopted the same parameters for the motion estimation reported here. The algorithm was verified by passing in sets of two identical images, one of which was shifted by a known amount and checking that the shift was correctly detected. Further verification was achieved by comparing velocity estimates obtained from the algorithm with visual estimates found by counting pixels.

Finally, the mean surface speed of the lake was found by averaging the magnitudes of the computed velocity vectors. To avoid possible edge effects, only velocity vectors from the central region (at least 3 pixels inside the lake boundary) of the lake were included in the averaging.

An animation showing results of the motion tracking methodology described above (from rectified images to mean lake speed) is provided in the supplementary material for the electronic version of this manuscript.

3.4. Time-series analysis

As can be seen in Fig. 2, the mean surface speed time-series obtained are highly non-stationary. To evaluate the periodic components of the series with time, we therefore use a Morlet wavelet transform to produce spectrograms of the data. Our implementation of the Morlet transform is the same as that of Boichu et al. (2010). The mean speed data were interpolated to a uniform 1 s time step prior to the Morlet transform using simple linear interpolation.

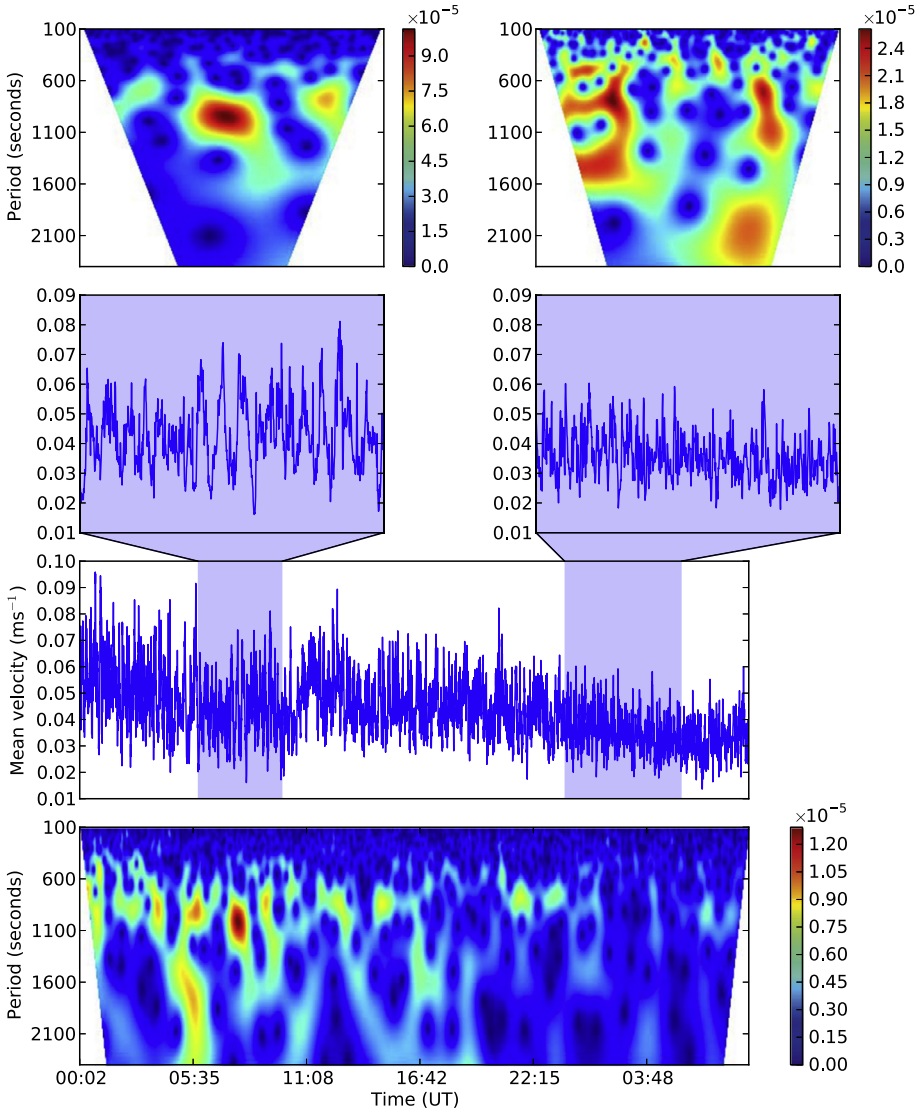

Fig. 2. Selection of mean surface velocity data from December 2010 and the corresponding Morlet wavelet transform showing the periodicities present. The expanded sections show how an increase in period is accompanied by an increase in amplitude. The colour scales represent the Morlet transform modulus.

As illustrated by the expanded regions in Fig. 2, some of the ∼5–18 min cycles are of much greater amplitude than others, and will result in a very high modulus in the Morlet transform. Longer time-series tend to exacerbate this problem, since they often contain at least a few very high amplitude oscillations, which then saturate the colour scale and mask much of the other detail. In this way, the cyclicity of the lake may not be apparent even if it exists. However, creating a spectrogram of just the data from the "non-cyclic" time period, reveals that there are indeed still ∼5–18 min period components present – they are simply of lower amplitude.

3.5. Bubbles

Bubbles breaking the surface of the lake manifest themselves as sharp peaks in the mean surface speed time-series. The poor time resolution of the Agema and P25 datasets mean that most bubbles are not recorded. However, much of the SC645 data from 2010 was recorded at 2 Hz, which is more than sufficient to capture the arrival of bubbles at the surface.

Bubble events were located in time by comparing the mean speed time-series to a low-pass filtered copy of itself. Bubbles were classified as events where the speed was greater than 1.2 standard deviations above the low-pass filtered value. The value of 1.2 was chosen by comparing bubble events detected by the algorithm to those located manually in a test set of data spanning three hours. The analysis was conducted on a continuous time-series of good quality data from 24 December 2010, spanning approximately 13 h. By visually inspecting the IR images corresponding to each of the bubble events, we determined that all events were small (metre-scale, with no ejection of material from the lake).

The bubble events detected are uniformly distributed in time. However, this tells us nothing of how they are related to the pulsatory behaviour of the lake. What is of real interest is how bubble events relate to the phase of the speed cycles; for example, do more bubbles surface during periods of fast surface movement? In order to evaluate a possible relationship between the cyclicity and bubble events we use the method of delays (e.g. Kantz and Schreiber, 2003) to reconstruct our time-series data into a phase space representation. If the bubble events are somehow correlated to the phase of the speed cycles then we argue that their distribution in phase space will differ from that of a random sample taken from the time-series. We can imagine this as being due to a clustering of bubble events at certain positions in phase space. Details of the phase space reconstruction are given in Appendix A where we show that in order to accurately represent our time-series, a 4-dimensional phase space (embedding dimension of 4)

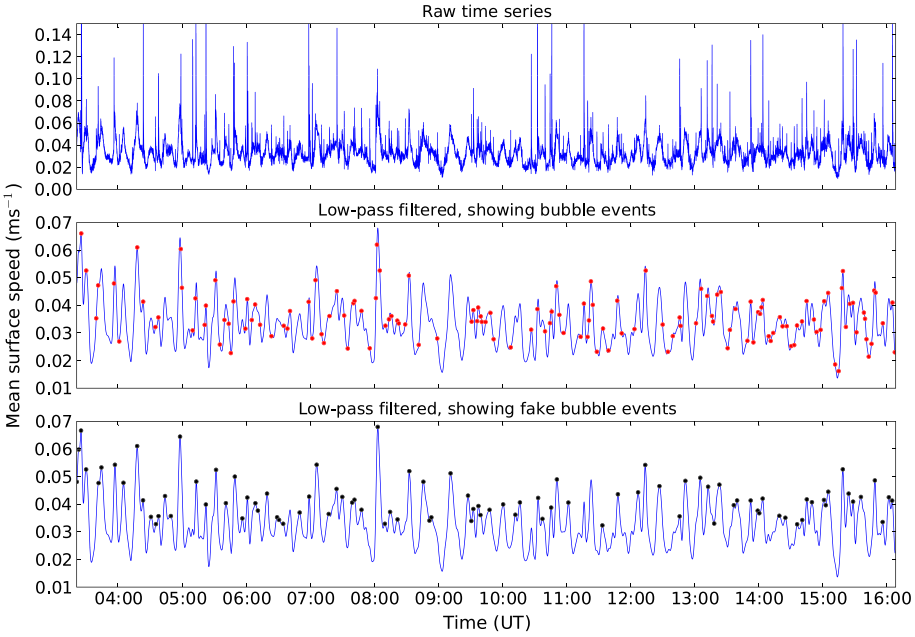

Fig. 3. Top panel: time-series of mean lake surface speeds from 24 December 2010. Middle panel: the same data, low-pass filtered to remove noise and spikes due to bubbles and with bubble events marked. Bottom panel: low-pass filtered data with the fake bubble events used for testing marked.

is required. The data were low-pass filtered prior to phase space reconstruction to remove noise and the spikes due to bubbles.

The time-series analysed contains 141 bubble events (Fig. 3). We compared the cumulative distribution function (CDF) of the bubble events to a reference CDF in each of the phase space dimensions. The reference CDF is the CDF of the time-series itself. As an indicator of the expected variation in CDFs, the standard deviation of 10,000 CDFs, each constructed from 141 points randomly sampled from the time-series, was computed. A significant variation of the bubble event CDF from that of the reference in any of the dimensions, would indicate some correlation to the phase of the cycle. Differences between CDFs were quantified using the two-sample Kolmogorov–Smirnov test (K–S test). The computed critical value for the K–S test at 90% confidence (based on a reference sample size of 90 901, and a bubble event sample size of 141) is 0.102.

To verify the technique, we created a set of 95 fake bubble events located at the peaks of the mean speed cycles (Fig. 3). These events were then subjected to the same analysis as the real bubble events. The critical value for the K–S test at 90% confidence is 0.125 for the fake bubble sample size of 95. As shown in Fig. 4, the CDFs for the fake bubble events show a strong deviation from that of the random samples in each of the phase space dimensions, with K–S test results of 0.50, 0.15, 0.16 and 0.13 respectively (i.e. all above the critical K–S value, suggesting the two samples came from different distributions). Hence, the technique correctly identified the correlation between the fake bubble events and the phase of the speed cycles.

4. Results

The 2010 field season was characterised by exceptional visibility of the lava lake. In addition to the IR images captured, several short time-series of visible images were captured using a digital SLR camera equipped with a telephoto lens. Fig. 5 shows a short time-series of mean surface speed and mean surface temperature data calculated from IR images, with visible images corresponding to peaks and troughs in the speed also shown. There are no consistent differences observed between the appearance of the lake surface during periods of high speeds and periods of low speeds.

Oppenheimer et al. (2009) found a strong correlation between the phase of cycles in mean surface speed and radiative heat loss in their data set. This correlation is further demonstrated by the time-series shown in Figs. 5 and 6. Note however, that since we have not attempted an accurate temperature calibration of the IR images, we present mean surface temperatures normalised to their maximum value. What is not clear from these data alone, is whether the temperature variations observed are due to an increase in the surface temperature of the lava in the lake, or an increase in the area of cracks in the surface crust of the lake caused by the increased motion (Oppenheimer et al., 2009). Additional cracks will expose more of the underlying lava to the surface and will therefore cause an increase in the mean temperature recorded by the IR camera. Increased cracking during periods of higher surface speed is not obvious in the images shown in Fig. 5, suggesting that the changes in recorded temperature are indeed due to variations in the mean temperature of the lake surface. However, we feel that a qualitative argument such as this is insufficient to rule out increased cracking as a cause.

In an attempt to identify more rigorously the reason for the temperature cycles, we compared the histograms of the thermal images at the minima and maxima of the cycles. If the cycles are caused by an increase in surface temperature, then we would expect the histograms at the cycle maxima to be shifted relative to those at the minima. If increased cracking is the cause, we would expect more high temperature pixels, resulting in a skewing of the histograms at the maxima compared to those at the minima. Unfortunately, the results obtained were ambiguous, with greater differences between histograms from the same point in the cycles than found by comparing those at maxima to those at minima. The cause of the measured temperature fluctuations remains elusive, however, it seems likely that they are caused by a combination of both increased surface cracking and increased surface temperature.

It is important to realise that even if increased surface cracking is insignificant, cycles in the surface temperature do not necessarily reflect periodic variations in the internal temperature of the lake itself. It is possible for example, that during periods of increased surface motion the mean surface age of the lake is lower. Younger crust is likely to be thinner, and hence the conductive heat flow through it will be larger, resulting in higher measured surface

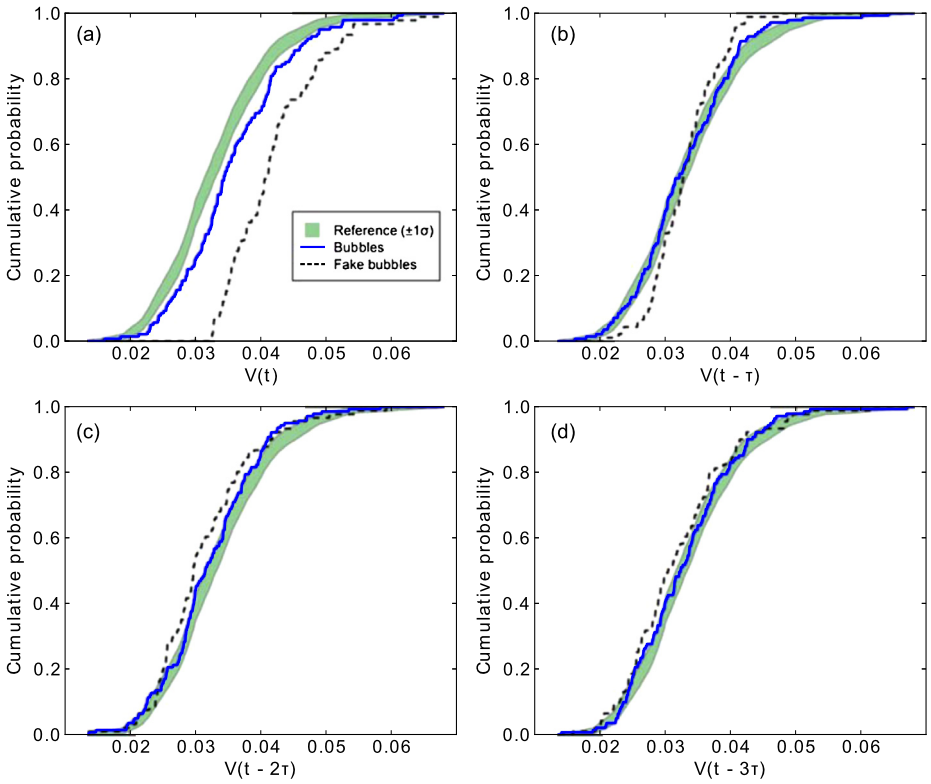

Fig. 4. The cumulative distribution functions (CDFs) in each of the four phase space dimensions for the bubble events (solid line) and fake bubble events (dashed line). The *x*-axes represent the coordinates of the events in the corresponding phase space dimension, from the zero-lags dimension, $V(t)$, up to the three-lags dimension, $V(t-3\tau)$, where $\tau = 150$ s (see Appendix A). The shaded region represents one standard deviation on either side of the reference CDF (i.e. the CDF of the mean speed data). Large deviations from the reference CDF are indicative of a correlation with the phase of the speed cycles, as can be seen in the fake bubble data. The deviation from the reference in the first dimension (a) of the bubbles CDF is attributed to imperfect filtering of the signal rather than a phase dependence.

temperatures despite the bulk temperature of the lake remaining static.

Fig. 6 shows a short time-series of mean surface speed and mean surface temperature calculated from IR images captured in 2010. The pulsatory behaviour was particularly pronounced during the period shown, and the waveform of the cycles is clear. The peaks in speed and temperature are approximately Gaussian in shape, with rising and falling edges that are symmetric about the centre of the peak. The peaks tend to be shorter lived than the troughs, suggesting a system with a stable baseline state that is being perturbed, rather than a system that is oscillating about a mid-point. There also appears to be a correlation between the magnitude of the cycles and their period, with longer period cycles having a greater amplitude. However, such a relationship is not always observed, and there are many instances where the opposite is true.

Morlet spectrograms of the mean speed data from the 2007–2011 field seasons are provided as supplementary material to the online version of this article. What is clear from the data is that the cycles in speed are not strictly periodic. Instead, there tends to be a broad range of periodic components present, centred at around 900 s. However, these components appear to be fairly consistent across the dataset and have not changed appreciably during the period of study. Fig. 7 further illustrates this point, showing the time average (normalised to have a mean of zero and standard deviation of one) of the modulus of all the Morlet spectrograms from each field season. The general trend towards higher modulus at longer periods is due to the fact that long period variations in mean speed tend to be of greater amplitude than short period variations (as is typical for most time-series data from natural systems). Despite this, the broad peak around 900 s is evident in the data from the 2007–2011 field seasons. The time-series from the 2004 and 2006 field seasons were of insufficient duration to allow analysis for long period behaviour, and as a result do not show the same behaviour as the other years.

It is unfortunate that during the 2005 and 2006 field seasons, which covered the period of increased explosive activity, IR data were either not collected at all, or are of insufficient length to compare to other years. However, as shown in Fig. 8, the pulsatory behaviour of the lake appears to be unperturbed by large bubble bursts. The figure shows a short time-series of mean surface velocity data from 29–30 December 2010, during which a large (∼30 m) bubble arrived at the surface of the lake. Despite a significant ejection of material from the lake, the mean speed data show that the pulsatory behaviour appears to be uninterrupted on timescales greater than that of lake refill (several minutes). It is interesting to note that at the time of the explosion, the Morlet spectrogram shows a particularly strong periodic component at ∼1000 s. We believe that this may be caused by increased surface speeds in the build-up to the explosion and also during the recovery phase as the lake refills. The IR images show that the lake level rises rapidly immediately prior to a large bubble reaching the surface, likely causing an increase in the recorded surface speed. Rapid flow of lava into the lake during the refill phase of an explosive event is also likely to cause elevated surface speeds.

In addition to the apparent stability of cycles in surface speed, the magnitude of the surface speed has also remained approximately unchanged since 2004. Although the mean surface speed can exhibit considerable variability (∼3–20 $\mathrm{cm\,s^{-1}}$) on a timescale of days, no systematic change was observed over the period of study.

Whilst the behaviour of the mean surface speed has remained remarkably stable, the visual appearance of the lava lake has changed significantly. Fig. 1 shows how the surface area of the lake

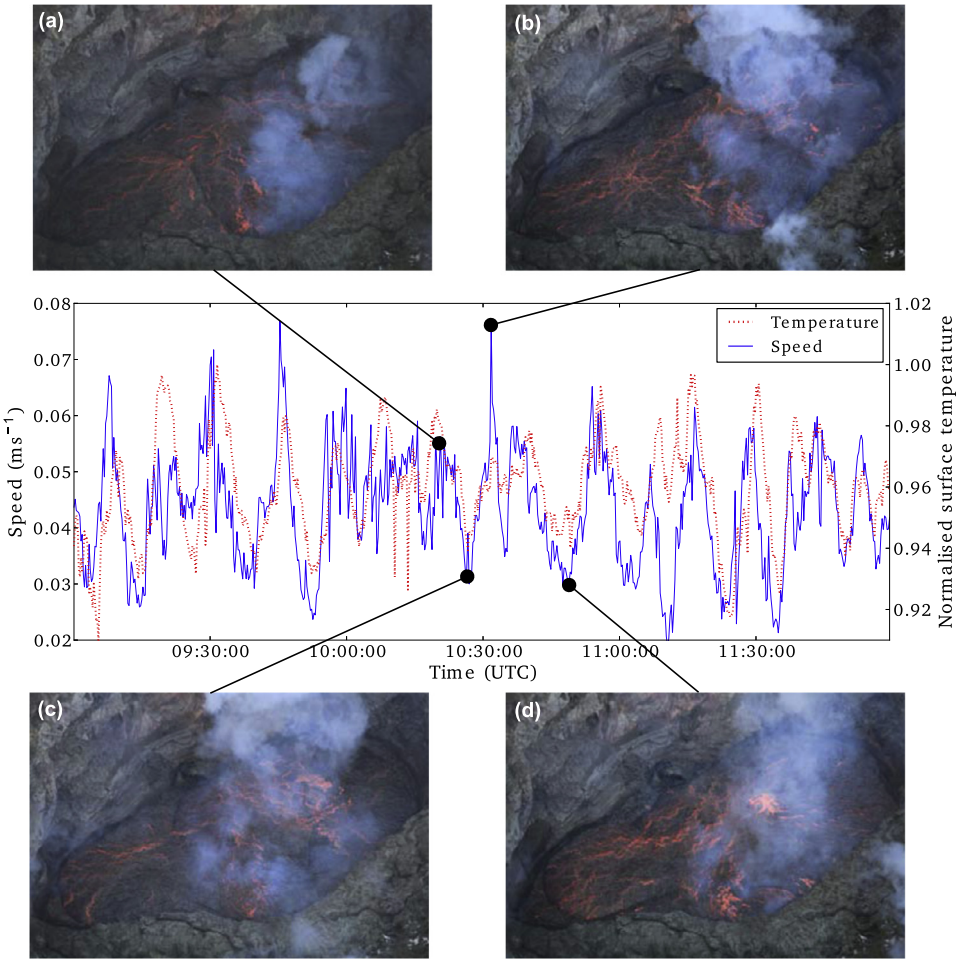

Fig. 5. Time series of mean lake surface speed and mean surface temperature (arbitrary units) from 17 December 2010 calculated from images captured with the P25 IR camera, with photographs showing the appearance of the lake surface at periods of high surface speed (a, b) and low surface speed (c, d). There is no distinct difference between the appearance of the lake surface during periods of high or low surface motion. Note that in (d), a small gas bubble can be seen just reaching the surface. Note that the bubble does not appear as "shot noise" in the speed data because of the poor time resolution of the P25 camera. The lake is approximately 40 m across its long axis.

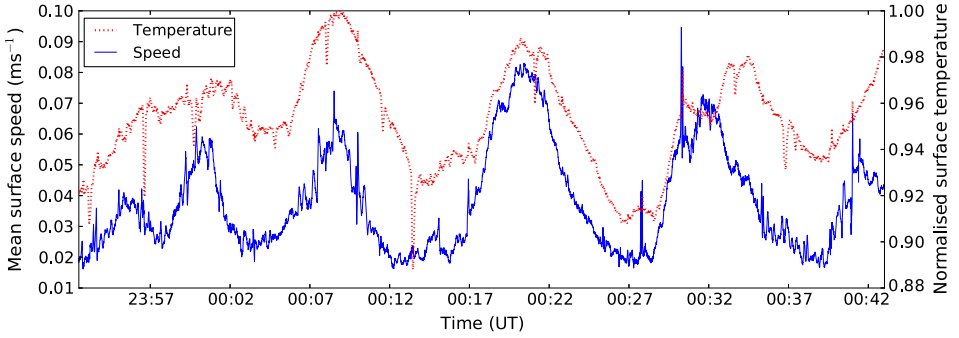

Fig. 6. Short time-series of mean surface velocity and mean surface temperature data from 21–22 December 2010 calculated from images acquired with the SC645 camera. We have not attempted to retrieve accurate temperatures from the images, and instead report unitless temperature values normalised by the maximum value in the time-series. The pulsatory behaviour is particularly clear during this period, and the symmetry of the peaks in time (i.e. about their horizontal centre) is evident.

(calculated from IR images and terrestrial laser scan data) has decreased since the first measurements in 2004. Overall the surface area has reduced by a factor of approximately four. The terrestrial laser scan data also show that since at least 2008 (when the first such data were recorded), the decrease in area has been accompanied by a 3–4 m per year drop in the lake's mean surface elevation (Jones, 2013, Frechette and Killingsworth, pers. comm.). The dramatic reduction in surface area cannot be accounted for by the drop in surface elevation (i.e. due to the lake receding into a conical basin) since the lake walls are observed (from terrestrial laser scan data and visual observations) to have a near-vertical profile. It seems likely therefore, that the observed decrease in surface area is due to a change in the geometry of the lake basin, either due to accretion of lava onto its sides, or deformation of the surrounding rock. The apparent lack of influence of lake geometry on the cyclic behaviour would tend to suggest that the cycles are driven by processes occurring in the magma conduit or a connected reservoir rather than in the lake itself.

Fig. 4 shows the cumulative distribution functions (CDFs) of the bubble events, and fake bubble events, in each of the four phase

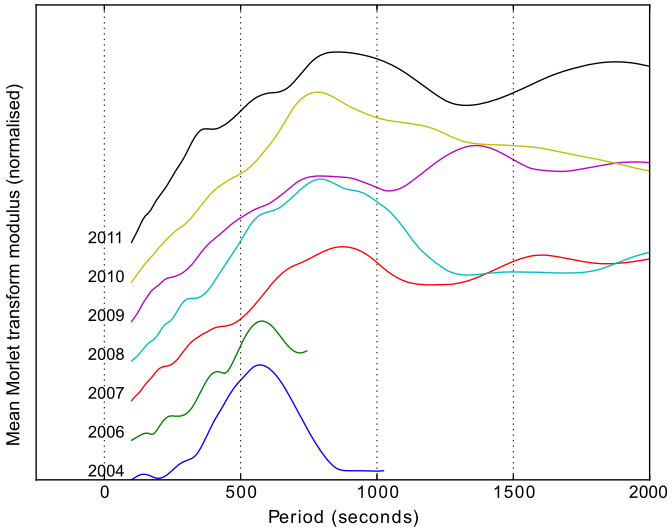

Fig. 7. Normalised time averages of the Morlet transform modulus of all available data from each field season. The data from each year have been vertically offset from each other for clarity. A broad peak corresponding to the period of the lake cycles (∼900 s) is evident in the 2007–2011 data. The time-series from the 2004 and 2006 field seasons were of insufficient length to be able to resolve long period fluctuations.

space dimensions. The shaded areas delimit one standard deviation on either side of the reference CDFs. As discussed in Section 3.5, the CDFs for the fake bubbles show a strong deviation from the reference, correctly identifying the correlation between the phase of the speed data and the fake bubble events. In contrast, the CDFs for the real bubble events are very similar to the reference in all but the first dimension. The K–S test gives values of 0.15, 0.05, 0.07 and 0.06 for the four dimensions, respectively. Apart from the first dimension, these are all below the critical K–S value at 90% confidence (0.102), indicating that the bubble events are from the same distribution as the speed data itself and that there is, therefore, no correlation between the phase of the speed cycles and the bubbles.

In the first dimension, the CDF of the bubble events appears to be the same shape as that of the mean speed data, but shifted slightly to the right (higher mean speed). We believe that this is caused by the failure of our low-pass filtering to remove fully the spikes caused by bubble events in the mean speed data, rather than any correlation with the phase of the cycles. As a result, bubble events appear to occur at slightly higher speeds than they actually do, shifting the CDF to the right. We tested this hypothesis by plotting the CDF of 141 randomly selected points from the speed data with a linear offset of 0.002 ms^{-1} added. The results showed a CDF that matched that of the mean speed data in all dimensions except the first, which showed a linear offset to the right as expected. We therefore conclude that the bubble events are not correlated to the phase of the velocity cycles and that the deviation we observe in the first dimension is due to the low-pass filter's inability to remove completely the effects of bubble events from the underlying mean speed signal.

5. Discussion

A common conclusion of multi-year studies conducted at Erebus volcano is that its behaviour is remarkably stable. Observations of radiant heat output (Wright and Pilger, 2008), SO_2 flux (Sweeney et al., 2008) and seismicity (Aster et al., 2003) have all found very little variation during the past decade. Our findings that the pulsatory behaviour of the lava lake has been a persistent and unchanging feature (both on a daily and a yearly time-scale) since at least 2004 fit well with these previous findings and further emphasise the remarkable stability of Erebus's magmatic system. The preservation of cycles in surface speed despite large perturbations to the system (decametric bubble bursts) is indicative not only of the stability of the responsible mechanism, but also that it is likely

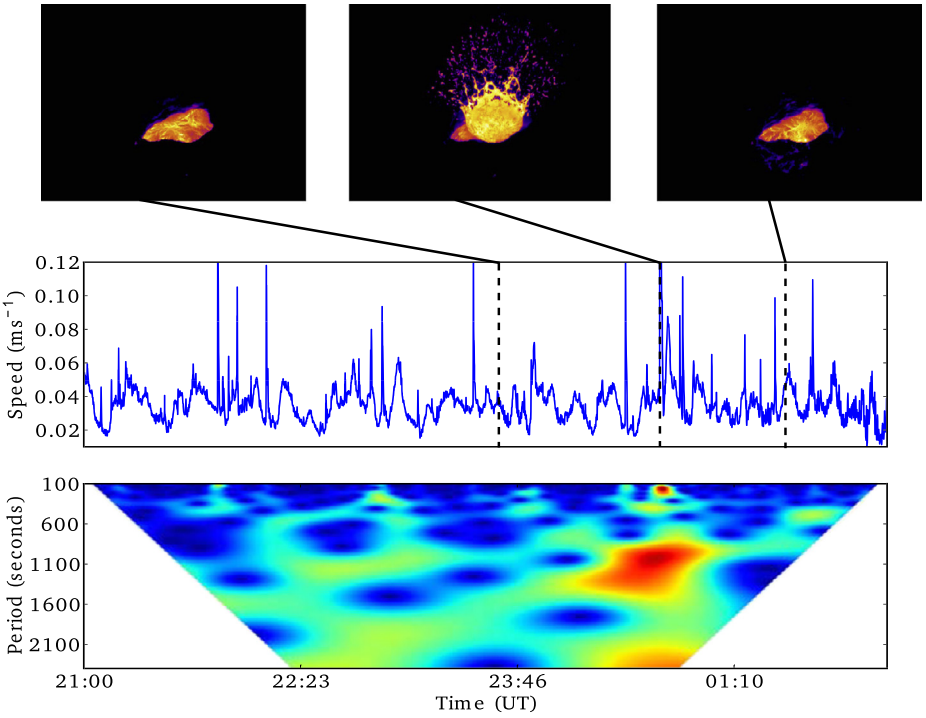

Fig. 8. A 5 h time-series of mean surface speed data from the 29–30 December 2010 calculated from images acquired with the SC645 camera and the corresponding Morlet spectrogram. The IR images above show the state of the lake before, during and after a large (∼30 m) bubble burst. Cycles of between ∼600–1100 s are visible across the time-series both in the Morlet spectrogram and in the mean speed data. The strong ∼1000 s signal in the spectrogram corresponding to the explosion itself may be caused by elevated speeds due to the rising of the lake level prior to the explosion and the subsequent refilling of the lake afterwards.

sourced at a deeper level than the lake itself. This argument is further supported by the consistency of the motion cycles despite a reduction in the area of the lava lake, exposed at the surface, over the period of observation.

The broad width of the peak in the spectrograms that we observe is consistent with the findings of Oppenheimer et al. (2009) who found the period of the fluctuations in mean lake speed to vary between ∼5–18 min for the 2004 dataset. Although short sections of our data appear to contain several discrete frequency bands within this range, such fine scale structure is never observed consistently over time periods of more than a few hours. No clear pattern to the variation of the period of fluctuations measured is evident from the spectrograms. However, it is important to consider how well the mean speed of the lake surface represents the underlying process responsible for the pulsatory behaviour. Even if this process contains well defined, discrete periods, complex flow dynamics and other forcing mechanisms (such as thermal convection within the lake) may result in a highly non-linear response in the surface speed. It is possible that the broad distribution in period of the cycles in speed observed is due to the complex coupling between a periodic driving mechanism and the dynamics of the bubbly flow within the lake. Given the correlation between surface motion and gas composition ratios (which must have different couplings to the driving mechanism) reported by Oppenheimer et al. (2009), we believe that the variability in period stems primarily from the variability in the underlying driving mechanism.

Current theories on driving mechanisms for lava lake fluctuations can be grouped into three main categories; (i) instability in density driven, bi-directional flow of magma in the conduit feeding the lake (Oppenheimer et al., 2009), (ii) "gas pistoning" caused by gas accumulation either beneath a solidified crust on the surface of the lake (Patrick et al., 2011) or as a foam layer at the top of the lava column (Orr and Rea, 2012), and (iii) gas bubble-driven pressurisation changes (Witham et al., 2006). In the latter mechanism, the (uni-directional) upflow of bubbly magma in the conduit is interrupted by excess hydrostatic pressure in the lake. Stagnation of the flow allows bubbles in the conduit to coalesce into large gas slugs that rise to the surface independently of the melt. The loss of large gas slugs at the surface of the lake causes an increase in pressure at the base of the conduit. If this exceeds the pressure in the magma chamber then downflow occurs, suppressing the ascent of bubbles in the conduit. As the lake drains, the downflow reduces until it can no longer suppress the ascent of bubbles, and the cycle repeats. Witham et al. (2006) were able to demonstrate this mechanism by bubbling air through a water column with a basin attached to the top to represent the lake. They observed cyclic variations in the depth of water in the basin, consisting of a logarithmic increase in depth followed by a rapid, linear decrease.

As shown by Orr and Rea (2012), gas pistoning, as observed at Kīlauea, is also an asymmetric process, consisting of a relatively slow, cumulative deviation from the baseline state of the system as bubbles are trapped in the foam layer or beneath the solidified crust, followed by a sudden release of the accumulated gas and rapid return to the baseline state. The temporal symmetry of the perturbations in the Erebus lava lake is not consistent with either of these mechanism. It may be argued that the complex geometry of the upper magmatic system of Erebus could lead to a more symmetric variation than observed by Witham et al. (2006) and Orr and Rea (2012). However, our finding that the arrival of small (metre-scale) bubbles at the surface of the lake is uncorrelated with the phase of the speed cycles is only consistent with the bi-directional flow mechanism. Both bubble-driven mechanisms require a periodic release of bubbles prior to lake draining and, in the case of the Witham et al. (2006) mechanism, a significant decrease in the number of bubbles during lake draining. Large (decametric) bubbles, typically occur at Erebus only a few times per week, and cannot therefore be responsible for the ∼5–18 min cycles. Since no periodic release of small bubbles is observed either (visually e.g. Fig. 5, or statistically Fig. 4), we argue that the pulsatory behaviour of the lava lake at Erebus volcano is driven by magma exchange between a shallow magma chamber (Zandomeneghi et al., 2013) and the lake via bi-directional flow in the connecting conduit.

It is interesting to note that, on average, bubble events in the data presented in Fig. 3 occur every 5.5 min. This is comparable to the cycles in surface speed, which range from ∼5–18 min in period. However, given that some cycles occur without any bubbles surfacing (e.g. 09:00–09:15 in Fig. 3) and given the random distribution of bubbles with respect to the phase of the cycles (Fig. 4), we believe the similarity in timescales to be coincidental.

Pulsatory behaviour deriving from bi-directional flow in a conduit has been demonstrated for single-phase systems using two fluids of different densities (Huppert and Hallworth, 2007). However, any exchange of magma occurring at the Erebus lava lake will clearly be multi-phase, and its dynamics will be influenced not only by the presence of gas bubbles but also by the large anorthoclase crystals which constitute 30–40% of the melt volume (Kelly et al., 2008). Indeed, numerical simulations of the Erebus magmatic system indicate that the inclusion of crystals has a very significant effect on the flow dynamics (Molina et al., 2012). While it is likely that gas bubbles play an even more significant role than the crystals, a complete multi-phase flow model of the Erebus system is not yet available. Whilst it is possible that the dynamics observed by Huppert and Hallworth (2007) may not be applicable to a complex multi-phase system such as that at Erebus, the lack of compelling evidence for an alternative mechanism leads us to conclude that instability associated with density-driven bi-directional flow is the most likely explanation for the observed cyclic behaviour. As noted by Oppenheimer et al. (2009), the density contrast driving the flow is likely to result primarily from magma degassing.

Bouche et al. (2010) observed that bubbles in the lava lake at Erta 'Ale volcano may be trapped beneath the cooled crust at the surface of the lake and forced to travel laterally until they encounter a crack in the crust before they can surface. If such a process were also occurring in the Erebus lake, then it would invalidate our comparison of the bubble events to the cycles in surface speed. The variable duration of lateral migration of bubbles would prevent any direct comparison of the timings of the bubble events and the phase of the cycles, since it would tend to randomise their arrival at the surface. However, it can be observed in the IR images that even small bubbles ($\ll$1 m in diameter) break the surface of the Erebus lake in areas with no visible cracks. We do not therefore believe that the crust on the Erebus lake inhibits bubble ascent, nor that it causes significant lateral displacement of bubbles. These differences likely reflect the contrasting rheologies of the magmas involved, which in turn reflect the differences in composition, temperature, viscosity and crystal content.

In our analysis of the correlation of bubble events to lake cycles (Section 3.5), we have only looked at small bubbles in detail, since the dataset did not contain any large events. Small bubbles may be sourced within the lake itself, whereas large (decametric, causing ejection of material out of the lake) bubbles are thought to have originated at greater depths (Oppenheimer et al., 2011; Burgisser et al., 2012). It is possible that the passage of large bubbles through the conduit may perturb the bi-directional flow of magma, causing variations in the period of lake surface speed fluctuations. Although no such variation was observed in Fig. 8, we do not believe this to be sufficient evidence to discount such a possibility. Since the arrival of large bubbles is relatively infrequent, a time-series spanning several months would need to be analysed to achieve a statistically significant sample size with which to

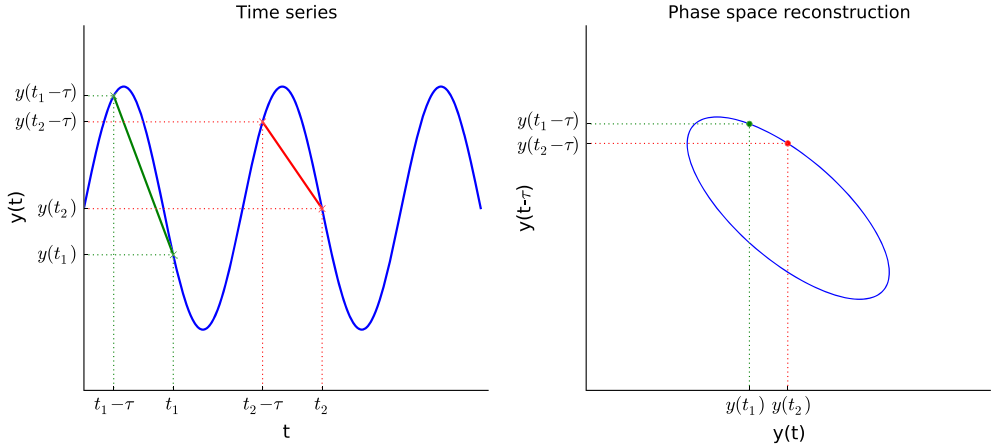

Fig. A.9. Phase space reconstruction of a simple time-series using the method of delays. The original time-series is shown in the left hand plot and the phase space reconstruction using a lag of τ and an embedding dimension of 2 is shown in the right hand plot. Samples from the time-series (e.g. t_1 and t_2) are mapped to phase space by plotting them against the value of the time-series one lag prior to their sample time.

investigate possible effects of large bubbles on the lake's motion. We are presently working on an autonomous camera installation on Erebus that we hope can provide such data (Peters et al., 2014).

6. Conclusions

We have reported an analysis of thermal infrared image data of the active lava lake at Erebus volcano that spans seven field campaigns from 2004–2011. In total 370,000 useful images were acquired representing 42 "field days" of observations and spanning contiguous observations of up to 44 h duration. The images were analysed using a feature-tracking algorithm to determine surface motion vectors from which the mean speed of the surface of the lake was derived, and this parameter used to monitor the lake's pulsatory behaviour. Shot noise in the mean-speed data was found to indicate bubbles arriving at the surface of the lake, allowing an analysis of the timings of bubble events with respect to the phase of the surface speed cycles.

Since 2004, the apparent size (surface area) of the Erebus lava lake has decreased by a factor of four. Despite these changes in the lake's appearance, its pulsatory behaviour has remained constant over the period of study, exhibiting cycles in mean surface speed with periods in the range ∼5–18 min. Mean surface speeds are typically between 3 and 20 cm s^{-1}. No obvious long-term progression of the cycles was observed. Surface speed time-series are not symmetrical about their mean (the troughs in speed are broader than the peaks), suggesting that the pulsatory behaviour is due to intermittent perturbations of the system, rather than an oscillatory mechanism.

Bubbles arriving at the surface of the lake show no correlation to the phase of the surface speed cycles. We therefore conclude that the pulsatory behaviour of the lake is associated primarily with the flow dynamics of magma exchange within the shallow plumbing system rather than by a flux of bubbles.

While we have analysed a substantially larger dataset than Oppenheimer et al. (2009), we have still been limited by the intermittent coverage. We hope that our recently-installed autonomous thermal camera system will yield much more extended time-series, facilitating investigations into the effect of large (decametric) bubbles on the pulsatory behaviour of the lake.

Acknowledgements

This project was funded by the European Research Council grant "DEMONS" (202844) under the European FP7, and the UK National Centre for Earth Observation "Dynamic Earth and Geohazards" theme (NERC NE/F001487/1: http://comet.nerc.ac.uk/). Field support was provided by the NSF under award ANT1142083. Terrestrial laser scan data were kindly provided by Laura Jones, Jed Frechette and Drea Rae Killingsworth. We wish to thank Alain Burgisser for his helpful comments on an early draft of the manuscript, and the two reviewers, Sylvie Vergniolle and Matt Patrick for their valuable suggestions.

Appendix A. Phase space reconstruction of mean speed time series

A clear description of the method of delays for phase space reconstruction is given by Kantz and Schreiber (2003) and also by Richter and Schreiber (1998). We will therefore not attempt to describe the technique in any detail here, instead we give the specifics of how the parameters required for delay reconstruction were calculated for our time-series. Essentially, phase space reconstruction of a time-series involves mapping each sample in the series to a vector in phase space. For a scalar time-series $x_1, x_2, x_3, \ldots$ the method of delays can be used to calculate the corresponding phase space vectors $\mathbf{x}_n = (x_n, x_{n-l}, x_{n-2l}, \ldots, x_{n-(d-1)l})$ where l is known as the lag, and d is the embedding dimension. Fig. A.9 shows an example of phase space reconstruction using the method of delays with an embedding dimension of 2, and demonstrates how points in the time-series are mapped into phase space.

Careful selection of both the lag and the embedding dimension is of paramount importance to obtain an effective phase space reconstruction of the original time-series. Estimation of a suitable lag for our data was performed using two different techniques. The first involved calculation of the autocorrelation function of the time-series. The time required for the autocorrelation function to decay by a factor of e is stated as being a reasonable estimate for the lag (Kantz and Schreiber, 2003). For our data, this gave a lag of 142 s. A second technique for lag estimation, also described by Kantz and Schreiber (2003), is to find the minimum of the mutual information of the time-series. We calculated the mutual information of our time-series using the TISEAN software package (Hegger et al., 1998), and found the minimum to be at 200 s. We repeated our bubble event analysis for several different values of lag between these two estimates and found no appreciable difference in the results. The results presented in this paper are from the analysis using a lag of 150 s.

To determine a good embedding dimension, we followed the approach proposed by Hegger and Kantz (1999), in which the false nearest neighbour method (Kennel et al., 1992) is combined with

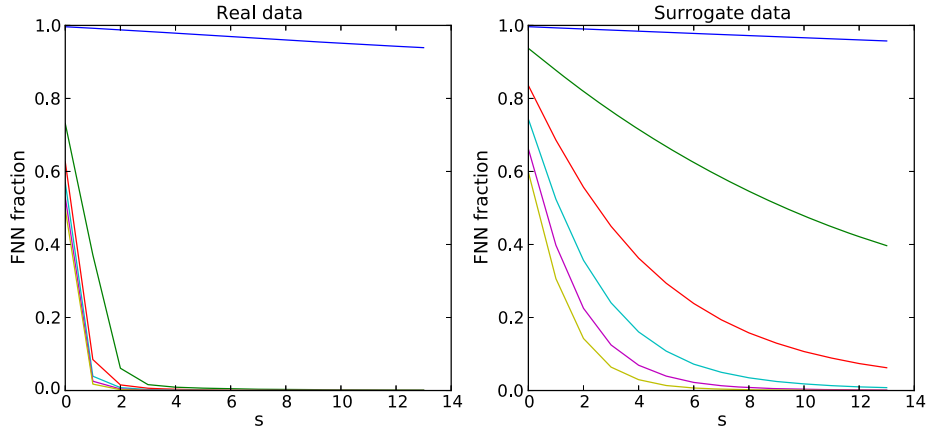

Fig. A.10. The fraction of false nearest neighbours (FNN) against the threshold value for embedding dimensions from 1 to 6 (top to bottom) and a lag of 150 s, for both the real data (left hand plot) and a surrogate data series (right hand plot). The difference between the real and surrogate data shows that the reduction in FNN as we increase the embedding dimension is not simply due to linear correlations in the data. For an embedding dimension of 4, the FNN fraction reduces very quickly for small threshold values and there is little difference in behaviour compared to larger embedding dimensions. We therefore chose 4 as a suitable embedding dimension for our analysis.

surrogate data tests. The false nearest neighbour method compares the ratio of distances between points and their nearest neighbours between an embedding dimension of n and $n+1$. If the ratio is greater than a threshold (s), the points are said to be "false neighbours". A high percentage of false nearest neighbours is indicative of too low a choice for the embedding dimension. The TISEAN software package was used both for the calculation of false nearest neighbours and for the creation of surrogate data (Schreiber and Schmitz, 1999). Fig. A.10 shows the calculated percentage of false nearest neighbours for different embedding dimensions and thresholds. There is a clear difference in behaviour between the real data and the surrogate data. This indicates that the loss of false neighbours as we move to higher embedding dimensions is not simply due to linear correlations in the data. Furthermore, we can see that, for an embedding dimension of 4, the percentage of false nearest neighbours falls away very rapidly for low threshold values. We therefore used 4 as our embedding dimension when performing the phase space reconstruction.

Appendix B. Supplementary material

Supplementary material related to this article can be found online at http://dx.doi.org/10.1016/j.epsl.2014.03.032.

References

Aster, R., Mah, S., Kyle, P., McIntosh, W., Dunbar, N., Johnson, J., Ruiz, M., McNamara, S., 2003. Very long period oscillations of Mount Erebus volcano. J. Geophys. Res. 108, 22. http://dx.doi.org/10.1029/2002JB002101.

Boichu, M., Oppenheimer, C., Tsanev, V., Kyle, P.R., 2010. High temporal resolution SO_2 flux measurements at Erebus volcano, Antarctica. J. Volcanol. Geotherm. Res. 190, 325–336. http://dx.doi.org/10.1016/j.jvolgeores.2009.11.020.

Bouche, E., Vergniolle, S., Staudacher, T., Nercessian, A., Delmont, J.C., Frogneux, M., Cartault, F., Le Pichon, A., 2010. The role of large bubbles detected from acoustic measurements on the dynamics of Erta 'Ale lava lake (Ethiopia). Earth Planet. Sci. Lett. 295, 37–48. http://dx.doi.org/10.1016/j.epsl.2010.03.020.

Bradski, G., 2000. The OpenCV library. Dr. Dobb's J. Softw. Tools 25 (120), 122–125. http://www.ddj.com/ftp/2000/2000_11/opencv.txt.

Bradski, G., Kaehler, A., 2008. Learning OpenCV: Computer Vision with the OpenCV Library, 1st ed. O'Reilly, Media.

Burgisser, A., Oppenheimer, C., Alletti, M., Kyle, P.R., Scaillet, B., Carroll, M.R., 2012. Backward tracking of gas chemistry measurements at Erebus volcano. Geochem. Geophys. Geosyst. 13. http://dx.doi.org/10.1029/2012GC004243.

Calkins, J., Oppenheimer, C., Kyle, P., 2008. Ground-based thermal imaging of lava lakes at Erebus volcano, Antarctica. In: Volcanology of Erebus Volcano, Antarctica. J. Volcanol. Geotherm. Res. 177, 695–704. http://dx.doi.org/10.1016/j.jvolgeores.2008.02.002.

Davies, A.G., Calkins, J., Scharenbroich, L., Vaughan, R.G., Wright, R., Kyle, P., Castano, R., Chien, S., Tran, D., 2008. Multi-instrument remote and in situ observations of the Erebus Volcano (Antarctica) lava lake in 2005: a comparison with the Pele lava lake on the jovian moon Io. J. Volcanol. Geotherm. Res. 177, 705–724. http://dx.doi.org/10.1016/j.jvolgeores.2008.02.010.

De Lauro, E., De Martino, S., Falanga, M., Palo, M., 2009. Modelling the macroscopic behavior of Strombolian explosions at Erebus volcano. Phys. Earth Planet. Inter., 174–186. http://dx.doi.org/10.1016/j.pepi.2009.05.003.

Dibble, R., Kyle, P., Rowe, C., 2008. Video and seismic observations of Strombolian eruptions at Erebus volcano, Antarctica. J. Volcanol. Geotherm. Res. 177, 619–634. http://dx.doi.org/10.1016/j.jvolgeores.2008.07.020.

Divoux, T., Bertin, E., Vidal, V., G'eminard, J.C., 2009. Intermittent outgassing through a non-Newtonian fluid. Phys. Rev. E 79, 56204.

Francis, P., Oppenheimer, C., Stevenson, D., 1993. Endogenous growth of persistently active volcanoes. Nature 366, 554–557. http://dx.doi.org/10.1038/366554a0.

Gerst, A., Hort, M., Aster, R.C., Johnson, J.B., Kyle, P.R., 2013. The first second of volcanic eruptions from the Erebus volcano lava lake, Antarctica – energies, pressures, seismology, and infrasound. J. Geophys. Res., Solid Earth 118, 3318–3340. http://dx.doi.org/10.1002/jgrb.50234.

Giggenbach, W.F., Kyle, P.R., Lyon, G.L., 1973. Present volcanic activity on Mount Erebus, Ross Island, Antarctica. Geology 1, 135–136. http://geology.gsapubs.org/cgi/content/abstract/1/3/135.

Hegger, R., Kantz, H., 1999. Improved false nearest neighbor method to detect determinism in time series data. Phys. Rev. E 60, 4970–4973. http://dx.doi.org/10.1103/PhysRevE.60.4970.

Hegger, R., Kantz, H., Schreiber, T., 1998. Practical implementation of nonlinear time series methods: the TISEAN package. arXiv:chao-dyn/9810005. Chaos 9 (1999) 413.

Huppert, H.E., Hallworth, M.A., 2007. Bi-directional flows in constrained systems. J. Fluid Mech. 578, 95–112. http://dx.doi.org/10.1017/S0022112007004661.

Jones, L., 2013. Terrestrial Laser Scanning (TLS) observations of Erebus volcano, Antarctica: insights into the near-surface magmatic system. Ph.D. thesis. New Mexico Institute of Mining and Technology. http://www.ees.nmt.edu/outside/alumni/papers/2013t_jones_lk.pdf.

Jones, E., Oliphant, T., Peterson, P., 2001. SciPy: open source scientific tools for Python. http://www.scipy.org/.

Jones, K.R., Johnson, J.B., Aster, R., Kyle, P.R., McIntosh, W., 2008. Infrasonic tracking of large bubble bursts and ash venting at Erebus volcano, Antarctica. J. Volcanol. Geotherm. Res. 177, 661–672. http://dx.doi.org/10.1016/j.jvolgeores.2008.02.001.

Kantz, H., Schreiber, T., 2003. Nonlinear Time Series Analysis, 2nd ed. Cambridge University Press.

Kelly, P.J., Kyle, P.R., Dunbar, N.W., Sims, K.W., 2008. Geochemistry and mineralogy of the phonolite lava lake, Erebus volcano, Antarctica: 1972–2004 and comparison with older lavas. J. Volcanol. Geotherm. Res. 177, 589–605. http://dx.doi.org/10.1016/j.jvolgeores.2007.11.025.

Kennel, M.B., Brown, R., Abarbanel, H.D.I., 1992. Determining embedding dimension for phase-space reconstruction using a geometrical construction. Phys. Rev. A 45, 3403–3411. http://dx.doi.org/10.1103/PhysRevA.45.3403.

Kingsbury, N., 2001. Complex wavelets for shift invariant analysis and filtering of signals. Appl. Comput. Harmon. Anal. 10, 234–253. http://dx.doi.org/10.1006/acha.2000.0343.

Knox, H., 2012. Eruptive characteristics and glacial earthquake investigation on Erebus volcano, Antarctica. Ph.D. thesis. New Mexico Institute of Mining and Technology. http://www.ees.nmt.edu/outside/alumni/thesis.php.

Kyle, P.R., Meeker, K., Finnegan, D., 1990. Emission rates of sulfur dioxide, trace gases and metals from Mount Erebus, Antarctica. Geophys. Res. Lett. 17, 2125–2128. http://dx.doi.org/10.1029/GL017i012p02125.

Magarey, J., Kingsbury, N., 1998. Motion estimation using a complex-valued wavelet transform. IEEE Trans. Signal Process. 46, 1069–1084. http://dx.doi.org/10.1109/78.668557.

Molina, I., Burgisser, A., Oppenheimer, C., 2012. Numerical simulations of convection in crystal-bearing magmas: A case study of the magmatic system at Erebus, Antarctica. J. Geophys. Res., Solid Earth 117. http://dx.doi.org/10.1029/2011JB008760.

Moussallam, Y., Oppenheimer, C., Aiuppa, A., Giudice, G., Moussallam, M., Kyle, P., 2012. Hydrogen emissions from Erebus volcano, Antarctica. Bull. Volcanol. 74, 2109–2120. http://dx.doi.org/10.1007/s00445-012-0649-2.

Oppenheimer, C., McGonigle, A.J.S., Allard, P., Wooster, M.J., Tsanev, V., 2004. Sulfur, heat, and magma budget of Erta 'Ale lava lake, Ethiopia. Geology 32, 509–512. http://dx.doi.org/10.1130/G20281.1.

Oppenheimer, C., Lomakina, A.S., Kyle, P.R., Kingsbury, N.G., Boichu, M., 2009. Pulsatory magma supply to a phonolite lava lake. Earth Planet. Sci. Lett. 284, 392–398. http://dx.doi.org/10.1016/j.epsl.2009.04.043.

Oppenheimer, C., Moretti, R., Kyle, P.R., Eschenbacher, A., Lowenstern, J.B., Hervig, R.L., Dunbar, N.W., 2011. Mantle to surface degassing of alkalic magmas at Erebus volcano, Antarctica. Earth Planet. Sci. Lett. 306, 261–271. http://dx.doi.org/10.1016/j.epsl.2011.04.005.

Orr, T.R., Rea, J.C., 2012. Time-lapse camera observations of gas piston activity at Pu'u 'Ō'ō, Kīlauea volcano, Hawai'i. Bull. Volcanol. 74, 2353–2362. http://dx.doi.org/10.1007/s00445-012-0667-0.

Patrick, M.R., Orr, T., Wilson, D., Dow, D., Freeman, R., 2011. Cyclic spattering, seismic tremor, and surface fluctuation within a perched lava channel, Kīlauea Volcano. Bull. Volcanol. 73, 639–653. http://dx.doi.org/10.1007/s00445-010-0431-2.

Peters, N., Oppenheimer, C., Kyle, P., 2014. Autonomous thermal camera system for monitoring the active lava lake at Erebus volcano, Antarctica. Geosci. Instrum. Method. Data Syst. 3, 13–20. http://dx.doi.org/10.5194/gi-3-13-2014.

Polikar, R., 2010. The wavelet tutorial. http://users.rowan.edu/~polikar/WAVELETS/WTtutorial.html.

Richter, M., Schreiber, T., 1998. Phase space embedding of electrocardiograms. Phys. Rev. E 58, 6392–6398. http://dx.doi.org/10.1103/PhysRevE.58.6392.

Schreiber, T., Schmitz, A., 1999. Surrogate time series. arXiv:chao-dyn/9909037. Physica D 142 (2000) 346–382.

Sweeney, D., Kyle, P.R., Oppenheimer, C., 2008. Sulfur dioxide emissions and degassing behavior of Erebus volcano, Antarctica. J. Volcanol. Geotherm. Res. 177, 725–733. http://dx.doi.org/10.1016/j.jvolgeores.2008.01.024.

Tilling, R.I., 1987. Fluctuations in surface height of active lava lakes during 1972–1974 Mauna Ulu Eruption, Kilauea Volcano, Hawaii. J. Geophys. Res., Solid Earth 92, 13721–13730. http://dx.doi.org/10.1029/JB092iB13p13721.

Witham, F., Llewellin, E.W., 2006. Stability of lava lakes. J. Volcanol. Geotherm. Res. 158, 321–332. http://dx.doi.org/10.1016/j.jvolgeores.2006.07.004.

Witham, F., Woods, A.W., Gladstone, C., 2006. An analogue experimental model of depth fluctuations in lava lakes. Bull. Volcanol. 69, 51–56. http://dx.doi.org/10.1007/s00445-006-0055-8.

Wright, R., Pilger, E., 2008. Satellite observations reveal little inter-annual variability in the radiant flux from the Mount Erebus lava lake. J. Volcanol. Geotherm. Res. 177, 687–694. http://dx.doi.org/10.1016/j.jvolgeores.2008.03.005.

Zandomeneghi, D., Aster, R., Kyle, P., Barclay, A., Chaput, J., Knox, H., 2013. Internal structure of Erebus volcano, Antarctica imaged by high-resolution active-source seismic tomography and coda interferometry. J. Geophys. Res., Solid Earth 118, 1067–1078. http://dx.doi.org/10.1002/jgrb.50073.